Single-shot Excimer Laser Ablation of Thick Polymer Resists on Metallic Substrates

Jeff C. Wu
AMP Incorporated

Richard T. Williams
Anqi Wu
Hanli Liu
Charles W. Himes
Wake Forest University

ABSTRACT

Single-shot excimer laser ablation of polymer resists on metallic substrates has been developed and used for ultra-selective electroplating of metals. Conventional approaches to laser ablation by direct photochemical or thermal erosion of the polymer have etch rates too low for the thick resists and high line-speeds needed in metal plating. Furthermore, the nature of the substrate in metal plating presents a special challenge for clean removal of a dielectric surface layer. The physical basis for defining parameters of a successful method for single-shot ablation of thick polymers on metallic substrates are described. Computer models taking account of optical absorp tion profiles, thermal diffusion, and phase changes have given a reasonable predictive description of the ablation mechanism, confirmed by experiments. Polymer thicknesses up to 13 μm on metal substrates have been ablated by excimer lasers in a single shot of modest fluence, using the method described.

INTRODUCTION

Gold and other noble metals such as palladium are widely used in separable electrical interconnections because of their corrosion resistance and good electrical conductivity. Typically, noble metals are electroplated on contacts stamped from copper-based alloys which provide the mechanical strength, spring characteristics, and bulk conductivity required for the interconnection. A barrier layer such as nickel is plated over the base metal prior to gold plating to prevent interdiffusion of gold and copper. From the standpoint of connector performance, gold is needed only in the immediate area of physical contact. * Thus the cost of a connector can be significantly reduced by restricting the application of precious metals to the zones where they are actually needed. Various implementations of cell plating, tip plating, and mechanical masking are commonly used to achieve some selectivity in plating. Although significant savings of precious metals have been realized, the areas plated by such methods still exceed the minimum size needed to insure good contact. Contact printing of a plating resist can also provide selectivity, but is primarily applicable to flat parts. The selectivity is still limited by the resist viscosity and the feature sizes achievable on printing wheels. In the following, we describe physical issues that have been involved in developing an ultra-selective plating method based on patterned ablation of a resist layer.

CONVENTIONAL LASER ABLATION

Laser vaporization or ablative removal of materials is almost as old as lasers themselves. Metal cutting and medical surgical uses are two diverse examples that received

*A thin flash of gold may be applied to a wider area for primarily cosmetic reasons, if desired,

attention quite earl y. The prospects for application of laser ablation of polymer films in the electronics industry received a particular impetus around 1983, short] y after the commercial introduction of excimer lasers, when it was demonstrated that intense ultraviolet pulses are adept at removing polymer materials with precisely defined edges and depths.[1]

Continuing work has demonstrated the effectiveness of short pulses of excimer laser light in removal of optically prescribed areas of polymer layers.[2,3] The sharp edges and lack of charring in the cuts led to the suggestion that ultraviolet ablation is photochemical in nature rather than essentially thermal. Since ultraviolet photons absorbed in bonding-antibonding transitions are efficient bond-breaking agents, it was proposed that the polymer chains are broken into many smaller molecules with larger aggregate volume, producing almost explosive removal of the affected layer. [1-3] At the deep ultraviolet wavelengths (193 nm or 248 nm) used for most of the early ablation work aimed at electronic applications, the polymer absorption coefficients (α) are typically very high, of order $10^5 cm^{-1}$. Consequently, most of the laser energy is absorbed by a thin layer, typically 0.1 to 0.5 µm. Accumulated evidence now suggests that photochemistry plays less of a role, at least for wavelengths longer than 193 nm.[4-6] The main mechanism for ablation seems to be thermal, as at longer wavelengths, with some assistance from photochemical bond-breaking. The desirable traits of a sudden explosive removal appear to be primarily a consequence of the very high absorption coefficients encountered in polymers at ultraviolet wavelengths and of the typically short duration of excimer laser pulses compared to thermal diffusion times, so that a sharply defined thin layer of the polymer can be suddenly heated to very high temperature without much involvement of surrounding material.

The etch depth per shot is generally found to be a strongly saturating function of excimer laser intensity with 14 ns pulses at 193 nm, as shown for the example of Poly-(methyl-methacrylate) (PMMA) in Figure 1. The etch depth per shot increases linearly with fluence at first, but levels off quickly above about 0.4 µm.[1] A sharply limited etch depth can be an advantage if it is desired to stop the removal at a precise depth. It is a disadvantage if one wants to remove a thick layer in a single shot. For most polymers, the maximum etch depth per shot of excimer laser radiation at reasonably attainable energy densities is about 0.5 to 1 µm. The reasons for this limitation lie primarily with the high uv absorption coefficients of the polymers and short (10 ns) pulse duration of excimer lasers, i.e. the same factors giving the desirable crisp removal characteristics cited above.

For **a** = $10^5 cm^{-1}$, typical of polyimide for **L #** 308 nm (see Table 1), roughly 2/3 of the laser energy is deposited in the first 0.1 µm of the polymer. Moving at sonic velocity, the ablated material can travel at most 0.01 mm by the end of a 10 ns laser pulse, and that motion is directed mainly normal to the surface, i.e. in the path of the incoming laser beam. Because the ablated material cannot be cleared out within the pulse duration, it absorbs much of the incoming radiation, becoming superheated to a plasma that absorbs and eventually begins to reflect the remainder of the laser pulse. Most of the energy spent on superheating the ablated products is wasted. Furthermore, the higher the laser intensity, the sooner the plasma stage is reached, with consequent self-termination of the ablation. These factors are the fundamental origin of the strong saturation of etch depth per shot.

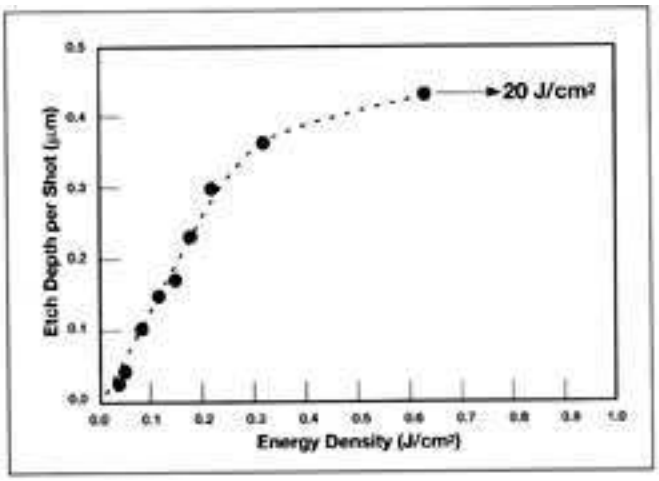

Figure 1. Etch depth per shot versus energy density for 14 ns, 193 nm pulses on poly-(methyl methacrylate). A pulse of energy density 20 J/cm^2 removed only 0.48 µm, emphasizing the strong saturation behavior. [From Ref. 1, by permission.]

Table 1. Absorption coefficients (in cm^{-1}) of selected polymers at ArF, KrF, and XeCl laser wavelengths. *

POLYMER	Wavelength 193 nm	248 nm	308 nm
Polyimide	4.2×10^5	2.8×10^5	1.2×10^5
Polysulfone	4.0×10^5	1.5×10^5	8.1×10^3
Novolac epoxy	1.0×10^5	2.1×10^4	2.4×10^3
Polycarbonate	5.5×10^5	1.0×10^4	2.2×10^3
Poly(α-methyl)styrene	8.0×10^5	6.5×10^3	8.0×10^2
Poly(methyl-methacrylate)	2.0×10^5	6.5×10^2	$<10^2$
Poly(vinylacetate)	1.0×10^5	$<10^2$	$<10^2$
Polyethylene	6.3×10^5	$<10^2$	$<10^2$
Polypropylene	5.3×10^5	$<10^2$	$<10^2$
Polytetrafluoroethylene (Teflon PET)	2.6×10^5	1.4×10^2	$<10^2$
Polyester			4×10^{3} (1)
Polyetherimide			$>4 \times 10^{3}$ (1)
Polyethersulfone	1.7×10^{5} (2)	6.1×10^{3} (2)	140 (2)

* From Ref. 12
(1) Our work
(2) Ref. 13

The most common way to increase cutting depth, as in industrial metal cutting applications, is to increase laser pulse duration and to provide an auxiliary method to remove vaporized or liquified material. However, now the immediate vicinity of the cut is raised to high temperature for a long period of time. The heat diffuses more deeply, and therefore

dissipates more slowly. Charring, distortion, or delamination may be the results when organic materials are involved and sharp definition is required. Furthermore, excimer lasers are primarily short-pulse devices. Long-pulse (200 ns) excimers are still mainly experimental, and the currently available pulse energy has been reduced with increasing pulse width. Thus presently available peak power scales roughly as the inverse square of pulse width and may fall below the ablation threshold, While long-pulse or cw lasers are fine for some forms of metal cutting, the above factors are significant drawbacks to using them for resists whose edges or critical bonding may be damaged, and substrates which may be damaged by excess heat and laser power. By choosing material/wavelength combinations to give somewhat lower absorption coefficients, the saturating etch depth can be extended in some cases to a few microns per shot. However, the desirable precision of excimer laser ablation seems necessarily to come at the price of an etch-depth limit of the conventional thermal/photochemical method.

REQUIREMENTS OF RESIST MASKING FOR ELECTROPLATING

Laser ablation offers the possibility of a process for selective plating by removing a well-defined area of a polymer resist before electroplating. Ablation is a noncontact process. As illustrated schematically in Figure 2, the definition of the patterns is obtained by mask imaging, so various geometries can be processed without using expensive tooling. A reasonable variety of laser wavelengths can be selected to match process parameters. The spatial resolution, which is determined mainly by the laser wavelength, is ample for most applications in electrical interconnections. Ablation of submicron lines in photoresist for semiconductor lithography applications and submicron drilling of molybdenum foil by excimer lasers has been demonstrated.[8]

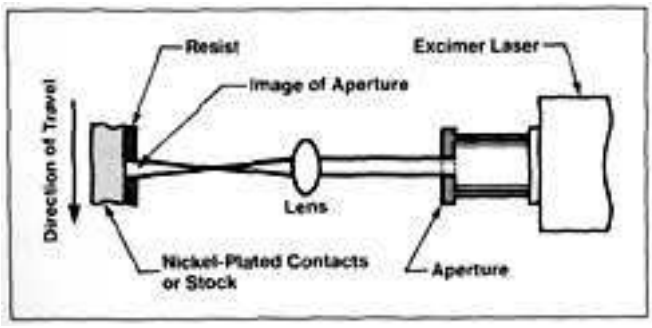

Figure 2. Illustration of set-up for selective masking of plating stock by laser ablation of resist as defined by a projected aperture image. The resist thickness is exaggerated.

In parallel efforts aimed at wafer-scale integration of active electronic components, the etch-depth limit may not be a significant problem. This could occur if thinner resists are used, or if intrinsically higher value per part makes the slower production speed associated with multiple shots per cut a viable option. However, in electroplating applications, the resist must be able to withstand rather harsh, agitated plating baths, implying substantial thickness. Furthermore, because of the nature of the parts and the production process, spin-on methods to insure uniform thin coatings are not applicable, so some form of spray or dip application must be used again, implying thick resists to insure complete coverage. The nature of the product often dictates a high line speed for economic feasibility, hence single-shot processes. Not only should the laser remove a large thickness of material, but it should do so uniformly in spite of any ripples or thickness variations in the applied resist, and should not overheat any part of the substrate. Furthermore, the nature of electroplating absolutely demands a cleanly exposed metal surface, with no residual polymer film. These were the basic challenges laid out for adapting laser ablation to electroplating.

An ultra-selective plating process using a XeCl excimer laser (308 nm) to remove a polymer resist has been developed and used in production. A plating resist with thickness between 2.5 µm and 13 µm has been used. A single shot from the laser removes the resist in a precisely defined area (Figure 3), subject to all the above requirements. The repetition rate is compatible with plating line speeds. This process is a novel approach to laser ablation of dielectric films on metal substrates, building on physical principles to be described in the following.

Figure 3. Contact cleared for selective plating by single-shot laser ablation. The ablated area is 500 x 750 µm (20 x 30 mils).

ELECTROMAGNETIC BOUNDARY CONDITIONS

In the above discussion, we raised the possibility of avoiding the etch-depth limit associated with excimer laser ablation by simply using longer wavelengths and longer pulses. Some problems with this were already outlined above, but in fact there are more. To understand a particularly important one, we need to consider the material combination involved in masks for electroplating. That is, we are necessarily dealing with a dielectric film on a metal substrate,

whereas much of the work in the literature has dealt with free-standing polymer films, or with insulator and semiconductor substrates. The difference lies in very fundamental requirements on an electromagnetic field (laser beam) at a metal-dielectric interface. For a perfect metal, the transverse electric field amplitude must vanish at the metal surface. A laser beam coming in at normal incidence will forma standing wave with a node at the metal surface. The electric field amplitude available to couple energy to the dielectric (assumed for the moment to have moderate absorption coefficient) increases from zero at the interface to the first maximum located at $\lambda/4$ above the interface. For CO_2 radiation, the closest maximum of the electric field to the metal surface lies in the polymer, about 2.5 μm from the interface. If the incident irradiance exceeds the ablation threshold by a factor of 2, there will still be a 1.2-μm layer of polymer adjacent to the metal that encounters subthreshold electric field amplitude and will not be ablated. This condition will not change substantially even on successive shots after the outer layers have been removed. This contributes to the fact, experimentally verified, that CO_2 laser pulses leave a thin polymer residue on metal that prevents good electroplating, even after exposure to 430 MW/cm^2 (13.6 J/cm^2 at 30 ns). The residual layer thickness determined by Auger spectroscopy and ion milling was on the order of 1 μm. Although the EM boundary condition on a tangential electric field is primarily responsible for the residue, another potentially important contributor is found in consideration of heat transport, to be discussed in the next section.,

In fact, the tangential electric field $E_{\parallel}$ outside a real metal with finite conductivity **s** does not vanish identically, but is reduced by the factor **d/l** relative to the applied field amplitude E_0. The classical skin depth is given by

$$\delta = c/\kappa\omega \qquad (1)$$

where κ is the imaginary part of the metal's refractive index, $\tilde{\eta} = n + i\kappa$, and **v** is the optical frequency.* Thus we find that the tangential field reduction is

$$E_{\parallel}/E_0 = \delta/\lambda = (2\pi\kappa)^{-1}, \qquad (2)$$

which may be directly determined from the optical constants of the metal. The rate of energy deposition is proportional to E^2, which for normal incidence of the light scales is $(E_{\parallel}/E_0)^2$. Examples are given in Table 2.1

It can be seen that the basic conclusions outlined above for a perfect metal interface still hold to a good approximation for most real metals and most optical frequencies. However, note that κ is a generally decreasing function of optical frequency, so that the tangential field reduction factor is generally less severe in the ultraviolet. In addition, the thickness of the low-field region decreases in proportion to the optical wavelength, since the first electric field maximum of the standing wave occurs at $\lambda/4$ above the metal interface. Even so, there is evidence in the literature that there still exists a problem for 488 nm light.[9] The observation arose in connection with investigations of optical data storage by ablation of a polymer on aluminized disks. About 40 nm of residual polymer remained after multiple laser shots. At 488 nm, aluminum is highly reflective, so that this case is similar to that already discussed for long wavelengths. The residual layer is very thin in this case, however.

As noted at the beginning, this problem ceases to exist if the substrate is an insulator or semiconductor. Unfortunately, this is no comfort to the electroplate.

HEAT DEPOSITION AND TRANSPORT

Not only does the EM boundary condition restrict the available electric field amplitude near the metal interface, but the high thermal conductivity of metals produces very effective heat-sinking of the adjacent polymer layer.

It is qualitatively self-evident that this is a problem. To be more specific than that, and to begin to deal quantitatively with questions of heating of deeper layers of metal, thresholds for ablation, angles of incidence, etc., we constructed a computer model of the ablation process, including heat transport in the substrate, optical energy deposition profiles in the polymer and the metal substrate, and phase changes in the polymer and substrate. The model is one-dimensional without significant loss of accuracy, because even for 250 μm (0.010-inch) feature sizes, the transverse dimension is at least 25 times the maximum relevant longitudinal distance, given by the thermal diffusion length

$$\ell = (k\tau/C)^{1/2}, \qquad (3)$$

where **t** is reasonably given by the laser pulse width, k is the thermal conductivity, and C is the heat capacity.

Thermal transport is treated by numerical integration of the one-dimensional heat diffusion equation with a source term:

$$\partial T/\partial t = k/C\ \partial^2 T/\partial x^2 + G(x,t)/C, \qquad (4)$$

The source term G(x,t) has a gaussian time dependence representing the laser pulse shape, and an exponential decay along x in accord with the absorption coefficient. The absorption profile is modified by a $\sin^2(2nx/L)$ envelope if the effect of standing waves produced by the EM boundary condition are being explored. Latent heats associated with phase transitions are taken into account on a slab-by-slab basis during the solution by finite differences. If the phase transition corresponds to vaporization, the affected slab and all slabs above it are removed.

Absorption coefficients for several polymers are listed in Table 1. In general, polymer absorption coefficients increase steadily with decreasing wavelength between 351 nm and

Table 2. Real and imaginary part of the refractive index (n, κ) and the skin depth **(d)** are listed for three metals at selected laser wavelengths. Also shown are the ratio $(E_{\parallel}/E_o)^2$ (see text) and (l–R), where R is the reflectivity.[14,15]

Metal	λ (nm)	n	κ	δ (nm)	$(E_{\parallel}/E_o)^2$	(1–R)
Ni	10600	7.400	39.305	42.92	1.63×10^{-3}	0.018
	1060	2.886	5.184	22.54	9.43×10^{-4}	0.275
	351	1.653	2.097	26.64	5.76×10^{-3}	0.576
	308	1.733	1.983	24.72	6.44×10^{-3}	0.608
	248	1.400	2.100	18.79	5.74×10^{-3}	0.551
	193	1.010	1.460	21.04	1.18×10^{-3}	0.655
Cu	10600	12.018	62.955	26.80	0.63×10^{-3}	0.011
	1060	0.358	7.067	23.87	5.07×10^{-4}	0.028
	351	1.297	1.896	29.46	7.05×10^{-3}	0.585
	308	1.350	1.710	28.67	8.66×10^{-3}	0.639
	248	1.470	1.780	22.17	7.99×10^{-3}	0.634
	193	0.970	1.402	21.63	1.25×10^{-2}	0.664
Al	10600	28.130	70.510	23.93	5.09×10^{-4}	0.0194
	351	0.327	3.916	14.27	1.65×10^{-2}	0.0765
	308	0.262	3.422	14.32	2.16×10^{-2}	0.0788
	248	0.172	2.700	14.62	3.47×10^{-2}	0.0794
	193	0.105	2.120	14.49	5.66×10^{-2}	0.0735

193 nm, due to the overlap of a number of spectrally broad electronic excitations associated with the valence bonding structure. In contrast, infrared absorption spectra are composed of many sharp features associated with specific vibrational modes. It is not as easy to generalize such spectra, but in most cases **a** is lower in the infrared than in the strong absorption region of the deep ultraviolet. Values for 10.6 μm measured in this work ranged downward from 600 cm^{-1}. Between the spectral extremes of infrared and ultraviolet, most pure insulating polymers are transparent, though a pigment may be added.

Energy absorption in the metal occurs within the classical skin depth **d** defined in equation (1), and has the magnitude (l-R), where the reflectivity R is given in terms of the complex refractive indices of metal, $\tilde{\eta}_m$, and polymer, $\tilde{\eta}_p$, as

$$R = \left| (\tilde{\eta}_p - \tilde{\eta}_m) / (\tilde{\eta}_p + \tilde{\eta}_m) \right|^2 \qquad (5)$$

or more simply for an air-metal interface as

$$R = \left[(n-1)^2 + \kappa^2 \right] / \left[(n+1)^2 + \kappa^2 \right] \qquad (6)$$

Values of (l–R) are tabulated in Table 2. As a general rule, (l-R) is very small for all metals in the infrared, and increases toward the ultraviolet, becoming quite material-dependent in the region of interband transitions, for example, in gold, copper, and nickel.

Figure 4 shows temperature profiles vs. time and position on both sides of the polymer/metal interface during the first shot and 2 successive shots of TEA CO_2 radiation at 13.6 J/cm^2, 30 ns duration. The resist is modeled on a styrene acrylate copolymer material used in corresponding laboratory experiments.[10] The polymer absorption coefficient at 10.6 μm was 325 cm^{-1}. The thermal parameters of nickel are k = 0.91 W/cm^3-°C and C_p = 5.017 J/cm^3-°C. In the figures, position (depth) is plotted with zero at the polymer/nickel interface, such that positions within the polymer are negative numbers. In Figure 4(a), the pseudo-three-dimensional temperature profile is viewed from the polymer side at late times to show the evolution of the polymer-air boundary as material is eroded. Starting at time zero in the back left corner, the rising temperature ramp in the polymer can be seen, culminating in an abrupt vertical drop after the vaporization temperature of 1000°C is reached. The drop to zero temperature is a graphical means of representing material removal in this format.

The model shows about 2 μm of polymer remaining after the first shot. There is a steep rise of temperature at the nickel interface due to direct heating of the metal, but the nickel temperature remains below 500°C. A plot of constant-temperature contours is shown above the pseudo-3-D representation. Although the contours are left unlabeled to avoid congestion, they occur at intervals of 10O°C and may be readily identified by projecting upward from the 3-D graph.

Figure 4(b) shows the first shot with the CO_2 laser as viewed from the nickel side of the interface at early times to show heating and cooling profiles more clearly. The plateaus on the polymer heating ramps indicate phase changes in progress. The temperature profile of nickel at the interface mimics the integrated laser energy with rapid cooling to the interior, whereas the polymer residue remains hot for a long time relative to the 100 ns time-scale shown.

Figure 4(c,d) shows the second and third shots on the same modeled spot, viewed from the polymer side. Only a thin additional polymer layer is ablated on the second shot, and nothing at all on the third. A permanent residue of about 1.9

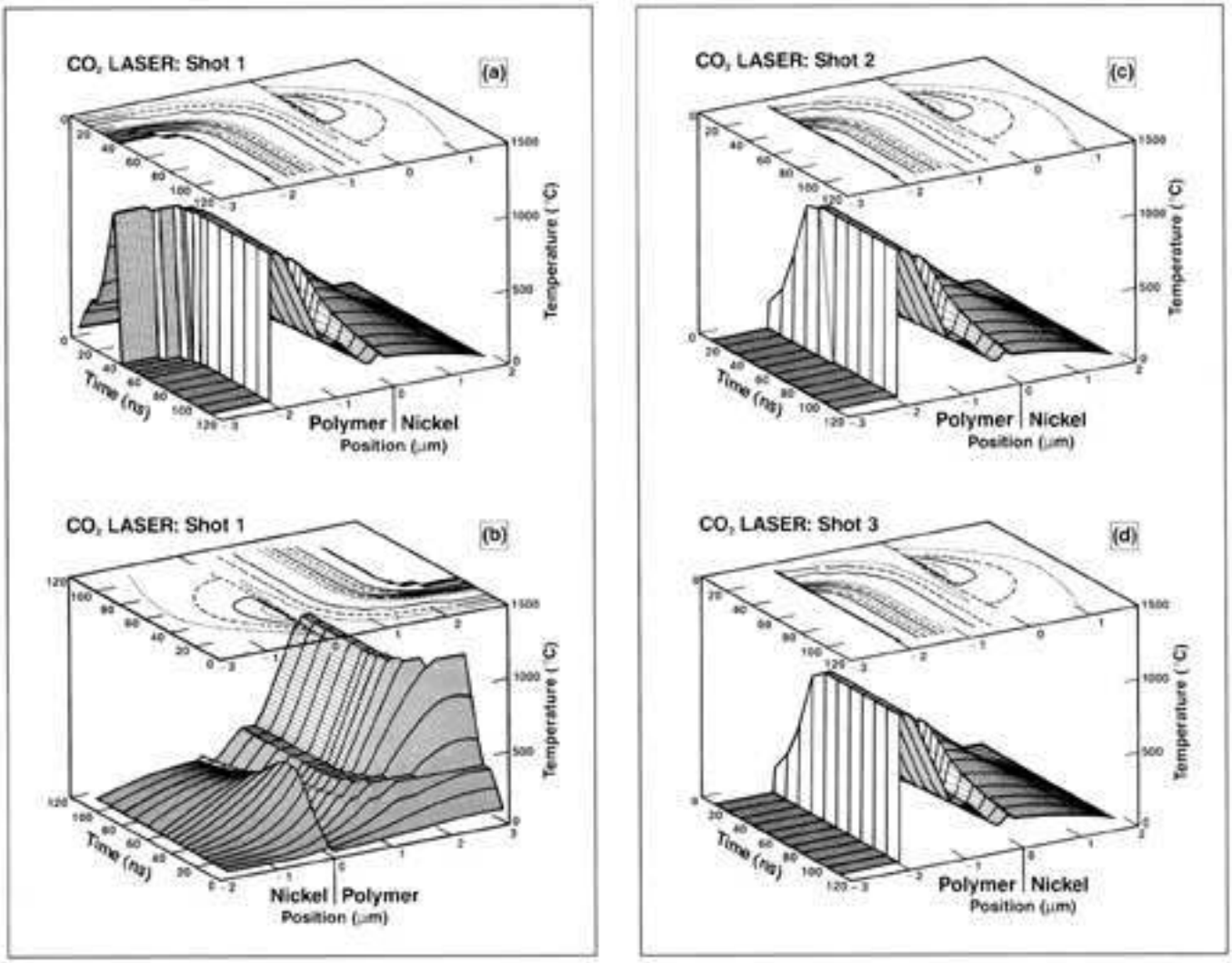

Figure 4. Temperature profiles vs. position and time for a styrene-acrylic copolymer on nickel at indicated times after exposure to a 13.6 J/cm^2, 30 ns CO_2 laser pulse. Position is measured normal to the film with zero at the polymer/nickel interface. Three successive pulses on the same spot are shown. Two perspective views of the profiles for the first shot are shown, as discussed in the text. The constant-temperature contours in the top plane are spaced at 100°C intervals and may be identified by comparison to the surface plot below.

μm is predicted for this case of CO_2 laser ablation. Corresponding laboratory samples were unplateable, with Auger profiles showing about 1 μm of polymer remaining.

Figure 5 illustrates the results calculated for the same acrylic polymer ablated by a KrF excimer laser (248 nm, 1 J/cm^2, 15 ns). At this wavelength, the polymer absorption coefficient is higher, $\mathbf{a} = 7 \times 10^3$ cm^{-1}. The computed behavior is quite different now, as shown in four views [Figure 5(a-d)] corresponding to those of Figure 4. About 1.5 μm of the original 3 μm of polymer is removed on each of two successive shots. (The stepwise material removal versus time within a single laser shot is an artifact of plotting a finite number of time profiles.) The metal substrate stays quite cool as long as it is shielded by the opaque polymer, but on the third shot [Figure 5(d)] it receives the 248 nm pulse directly. Because the metal reflectivity at this wavelength is much lower (see Table 2), the nickel temperature rises briefly to almost 1500°C on the third shot. The thin layer of polymer left at the interface remaining after the second shot is finally removed on the third shot, partly assisted by the high nickel temperature. A clean metal surface is revealed in Figure 5(d).

The results shown in Figure 5 were confirmed (including the inability to remove a layer of more than about 1.5 μm in a single shot) experimentally by samples which are cleanly plateable, showing no residue after a number of shots have impacted. The ability to remove the last residue of polymer comes both from the much shorter $\lambda/4$ characteristic of KrF radiation and from the more efficient coupling of uv light to the metal. This case corresponds to conventional excimer laser ablation of a polymer. It will be useful at this point to describe diagnostic measurements made during the laboratory experiments corresponding to this condition.

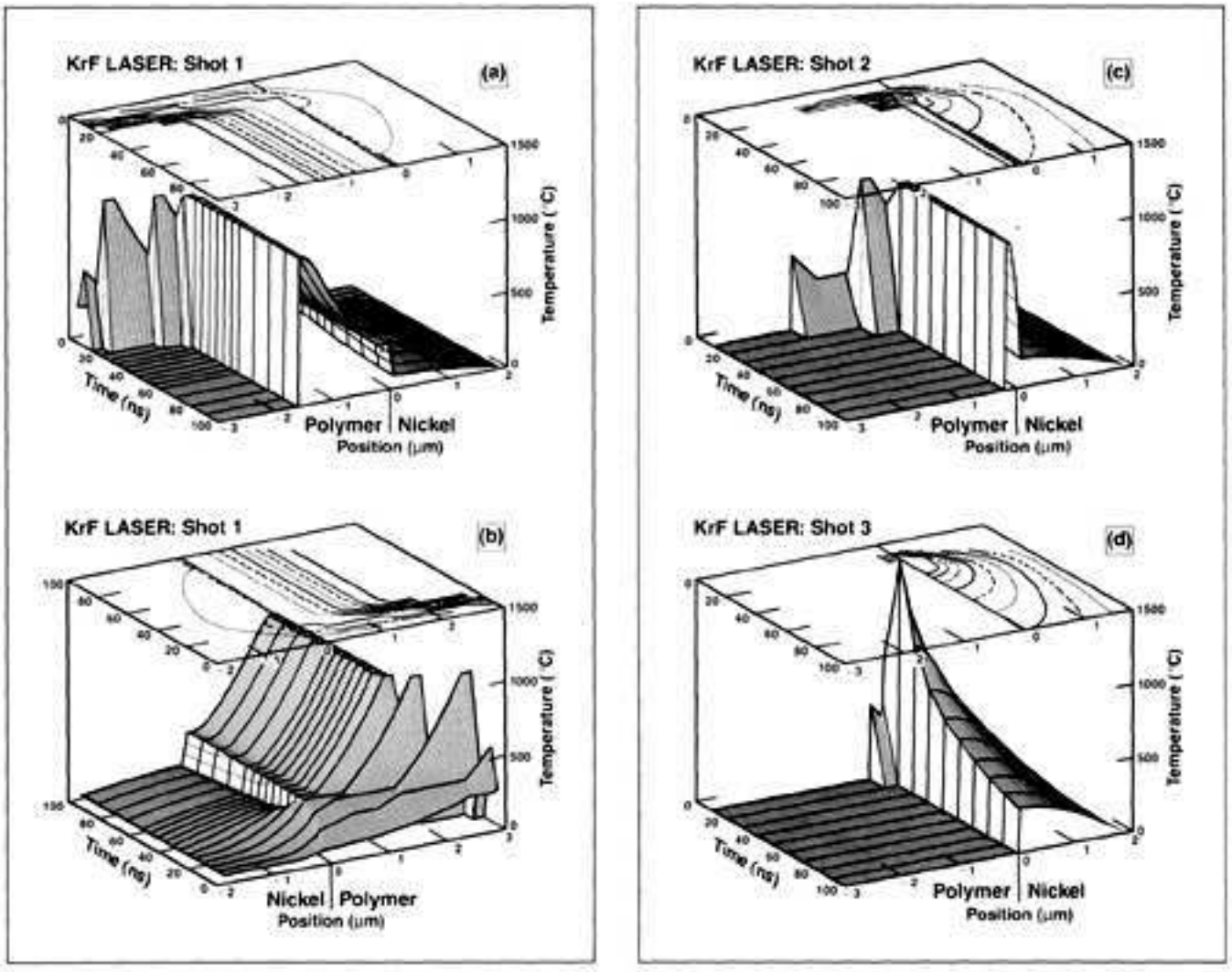

Figure 5. Temperature profiles of a styrene-acrylic copolymer on nickel at indicated times after exposure to a 1 J/cm^2, 18 ns KrF laser pulse. The pseudo-3-D and contour presentations of data follow the format discussed for Figure 4. Three successive pulses are shown, with two views of the first pulse.

Since the ablated material is superheated in this approach, as described earlier, each ablative shot is accompanied by an audible pop and flash, until the final layer is removed, at which time the process goes silent and there is only the faint blue glow associated with the nickel surface. The optical plume signature was quantified by measurement of the spectrum on each shot with an optical multichannel analyzer. Results are shown in Figure 6 for an acrylate polymer ablated at two wavelengths, 248 nm corresponding to higher absorption coefficient, and 351 nm corresponding to lower absorption coefficient. The sharp spectral lines are mainly identifiable with the Swan bands of C_2 and similar bands of CN. By analyzing vibrational populations evidenced in the spectra of Figure 6(a), we have determined that the vapor temperature reaches about 5300°C in ablation of the highly absorbing polymer at an energy density of 1 J/cm^2. At higher energy densities in the saturating part of the etch-depth/shot curve, emission lines of singly and doubly ionized carbon have been seen,[11] confirming the existence of a plasma in the saturation regime. Near the end of the shot sequence in Figure 6(a), the emission goes dark fairly suddenly, corresponding to the endpoint of the ablation process.

The optical spectrum in Figure 6(a) suggests that the acry - late polymer, for example, is broken into small fragments such as C_2, and/or reacted with air to produce species such as CN. We have performed mass spectrometry on the products of ablation, finding a range of small hydrocarbon fragments. Such work is useful to test for production of toxic vapors. The CN seen in optical spectra comes from reaction of carbon with nitrogen in the air under plasma or shock conditions associated with high-temperature ablation, and is found to the same degree around any carbon arc or plasma in air. Although such products are minority species, it is desirable to reduce them as much as possible. The process to be described below cuts the production of volatile products by more than a factor of 200 compared to conventional abla-

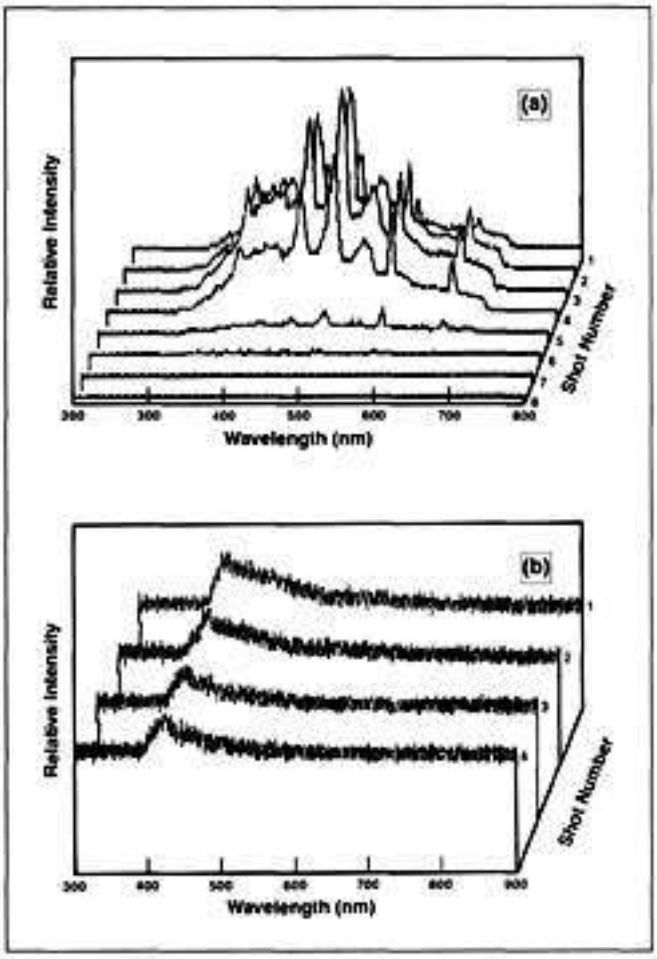

Figure 6. Optical spectra of an acrylate polymer ablated by successive pulses of laser light: **a)** KrF (248 nm) laser at 2 J/cm^2; b) XeF (351 nm) laser at 1.7 J/cm^2. In case (a), the polymer was entirely removed after 5 shots. In case (b), the polymer was entirely removed on the first shot, and the optical emission is mainly characteristic of the nickel metal surface.

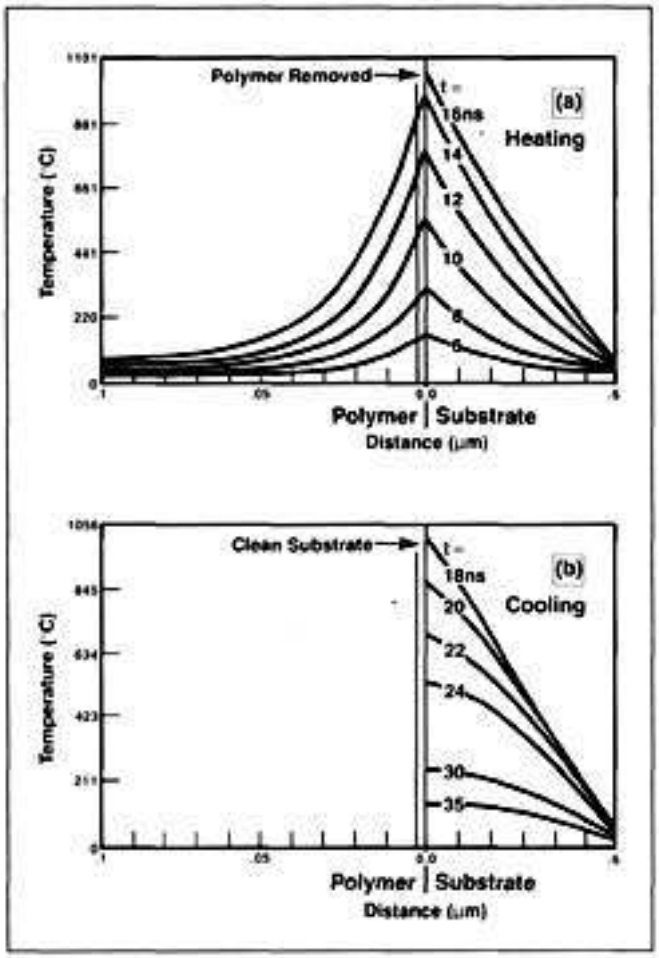

Figure 7. Temperature profiles of a styrene-acrylic copolymer on nickel at indicated times after exposure to a 0.6 J/cm^2, 10 ns XeF laser pulse. The upper plot shows profiles during heating, and the lower plot shows cooling profiles.

tion, simply by allowing most of the polymer to remain in solid phase throughout the removal.

"INSIDE-OUT" ABLATION

Figure 7 shows computed results for XeF laser radiation (351 nm, 1.0 J/cm^2, 10 ns) on a styrene-acrylic polymer with moderately low absorption coefficient, **a** = 670 cm^{-1}. Using the same modeling program, the results are plotted as a sequence of 2-D temperature versus position plots at a succession of times during heating and cooling. In a single shot, the entire 3 μm layer is removed. In laboratory trials under the same conditions, this result is verified even for much thicker polymers, up to 13 μm, without necessarily finding the limit. The same ablation process and results are found when XeCl laser light at 308 nm is used, for which **a** = 800 cm^{-1} in this polymer. In contrast to the conventional ablation described above, this event is very quiet with very little light emitted. Observing the process, one can easily see the polymer flying off in the form of a solid fragment. In the production environment, the fragments are drawn off in a rapidly moving air stream. To evaluate the process, we weighed a sample before and after ablation, and collected the solid fragments produced during ablation, which are primarily in the form of films or filaments (Figure 8). The results showed that more than 99.52% of the removed solid polymer remains in solid form, retaining the physical appearance of the polymer rather than changing to charred material. Electron-paramagnetic resonance performed on the ablation products showed no detectable formation of free radicals stable at room temperature. The molecular weight of the collected solid fragments was measured to be essentially the same as the molecular weight of the polymer before ablation. This further de-emphasizes the role of photochemical bond breaking, certainly for 308-nm light, and supports what appears to be essentially a pressure-induced mechanical shear as the mechanism for the process described.

The mechanism can be understood as follows. For absorption coefficient less than 800 cm^{-1} in a 3-µm film, more than 79% of the laser light is transmitted to the metal/polymer interface. As shown in Table 2, nickel absorbs 57.9% of the incident light at 308 nm, and does so within a very shallow depth of about 24.7 nm. As shown in Figure 7, this heats the nickel surface briefly to about 1100°C at the threshold for this ablation process. The slope of the temperature profiles at the interface in Figure 7 shows that the nickel transfers heat outward to the adjoining polymer, causing a thin layer to vaporize. The expanding vapor lifts off the outer layers in solid form, as illustrated in Figure 9. The styrene-acrylic polymer studied in this work has been shown to shear cleanly at the edges of the pattern, without lifting off from the surrounding metal.

The computer model and experiments agree that polymer ablation can be achieved without raising the nickel surface to its melting point. The window extends from the ablation threshold, roughly 0.6 J/cm^2 depending on polymer, up to the onset of nickel melting at about 1.2 J/cm^2. At the onset of nickel melting, the molten layer is extremely thin, and does not affect surface topography to any significant degree. At about 2.5 J/cm^2, the surface topography does change—it becomes significantly smoother. This laser polishing may have benefits in its own right.

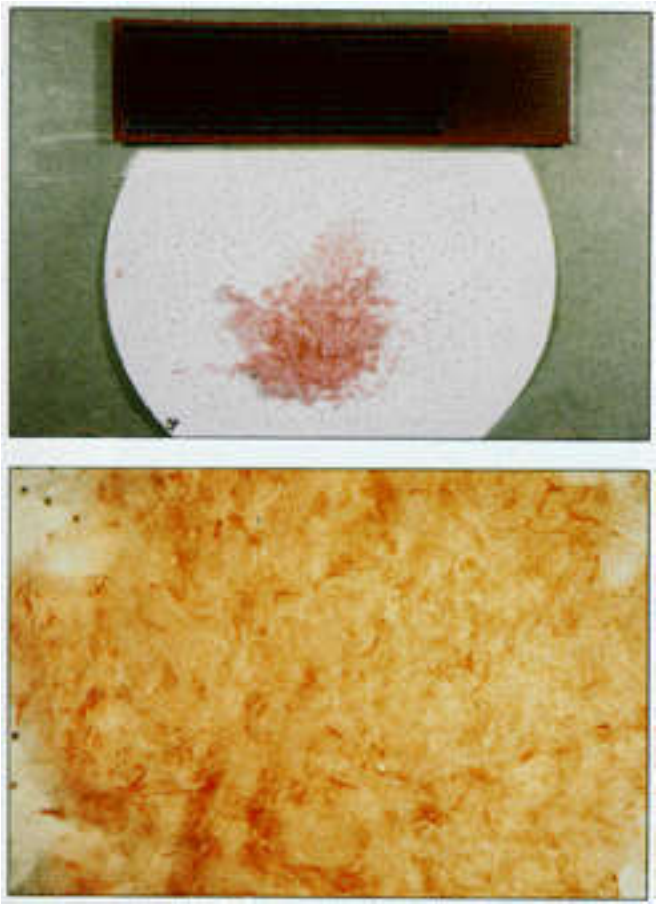

Figure 8. Polymer-coated strip a) with region ablated by inside-out mechanism described in text. Also shown are the collected solid fragments, which amount to 99.52% of the removed polymer weight. The close-up in b) shows the texture of the ablated polymer.

Also of concern are possible effects of deep heating of the spring alloy which makes up the strength member of the connector. Using the computer model, the temperature profiles versus time were investigated in 5 µm of nickel plated on 100 µm of phosphor bronze under irradiation by XeF (35 1 nm) and XeCl (308 nm) pulses including energy densities well above the threshold for polymer ablation. Figure 10 shows the results for an XeCl shot on nickel on bronze, where the zero of position is at the interface. During the 100 ns time-scale plotted, the bronze remained very cool, even though the nickel surface reached 2000°C. The maximum temperature at the nickel/bronze interface was 130°C, reached at 500 ns (not shown on this plot). No more than 15 µm of bronze ever rose above 100°C under these conditions.

To further confirm the basic mechanism, the following experiments were performed. A styrene-acrylic polymer with low absorption at 351 nm (and 308 nm) was coated on substrates of nickel, copper, aluminum, and quartz. Referring to Table 2, it can be seen that nickel and copper have low reflectivity, and thus high absorption, at 351 and 308 nm. In contrast, aluminum has high reflectivity, and thus low absorption, at these wavelengths. Quartz has low reflectivity and negligible absorption. The results were as expected on the basis of the model described above. The polymer was easily removed from nickel and copper, but was extremely difficult to remove from aluminum and quartz.

A high-speed framing camera was used to record successive 10 µs intervals after the laser shot to probe the dynamics of

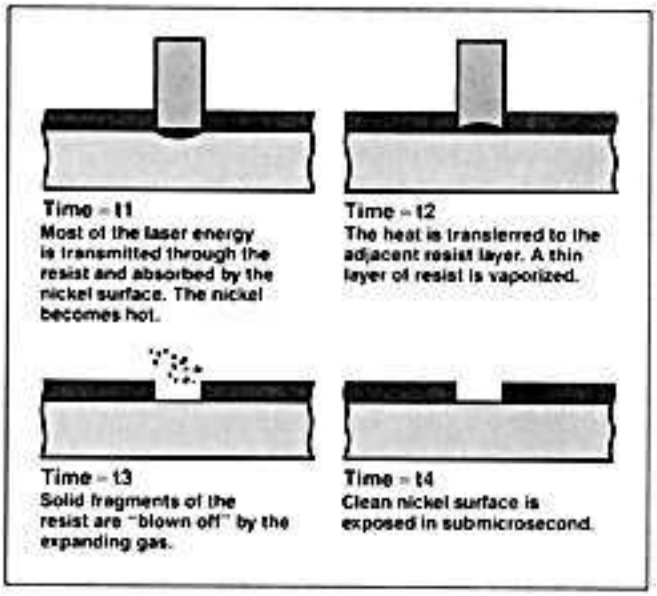

Figure **9.** Steps in ablative removal by the "inside-out" mechanism described in text.

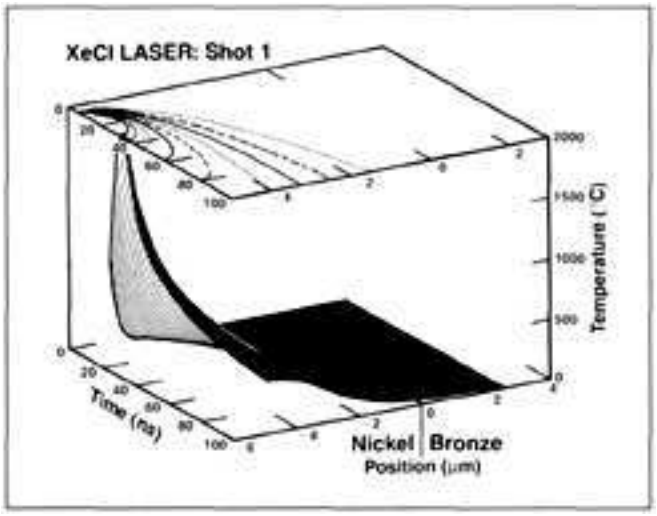

Figure 10. Temperature profiles of nickel plate on phosphor bronze after exposure to a 1.8 J/cm², 10 ns pulse of 308 nm light. The nickel/bronze interface is at position O, with nickel coordinates plotted at negative positions.

the resist-separation in real time. The first frame in Figure 11 includes the arrival of the 308-nm laser shot itself, showing the incandescent flash from the nickel and the small fraction of material which is vaporized. All successive frames were photographed in reflected light from a mercury arc. At 10 μs after the laser shot, a plume of vapor has blown past the solid film fragment, mainly around its edges, at a velocity of 341 m/s, about 99% of sonic velocity. The majority of the vapor cloud has already passed the solid fragment at this point, ending the acceleration phase and the fragment continues to move ballistically. At 30 μs, the end of the plume has stagnated and begun to form a mushroom, but the solid fragment, visible in reflected light as the bright spot at the left end of the plume, has moved only slightly.

After 30 μs, motion of the solid fragment can be discerned by comparison to the first frame. Fragment velocity at this point is 39 m/s, confirming that the average energy expended per unit mass removed is much lower in this process than in conventional ablation, where essentially the entire mass comes off in the high-speed plume. Knowing that about 99% of the removed polymer remains in solid phase, the squares of the velocities of plume and fragment can be compared directly to show that the energy expended is 76 times lower per-mass-removed in this "inside-out" ablation than in conventional decomposition to vapor phase.

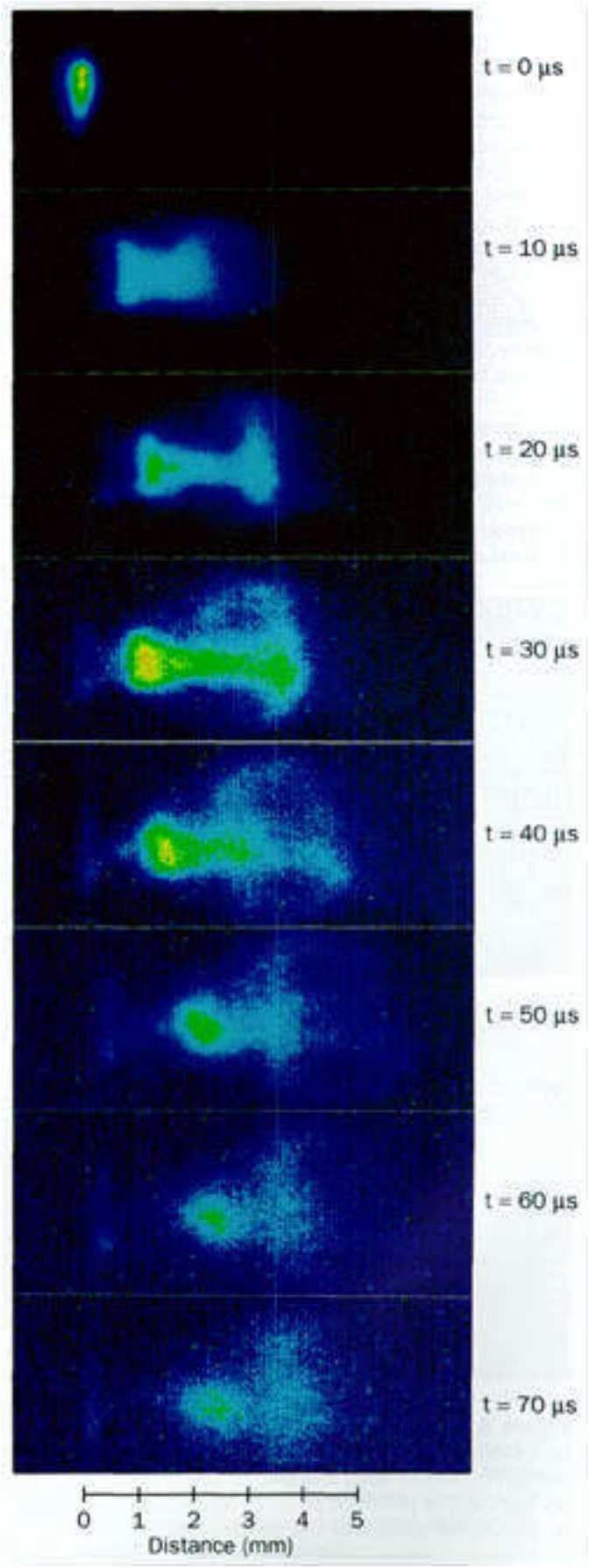

Figure 11. High-speed photographs of XeCl laser ablation of styrene-actylic copolymer by the mechanism described. Frames were captured at 10 μs intervals, under external illumination. The events are described in the text.

By 50 µs, the plume has largely dissipated, leaving the solid fragment still at its original size and moving at an average velocity of 40 m/s. At this point, the larger inertia/drag ratio of the solid fragment is causing it to close the gap on the remnants of the mushroom cloud. It will eventually pass through.

This paper has described only the physics of the ablation mechanism. The complete photomasking process also required the selection of appropriate polymers and the development of methods for applying them uniformly to the contacts at line speed. Synchronization and targeting of the laser pulses, removal of debris, and stripping the polymer after plating were essential steps.

ACKNOWLEDGMENT

Many people were instrumental in these developments, including C. Brooks, M. McCleaf, F. Vyas, D. Goetzinger, J. Joyce, J. Rowlette, and G. Clark. Advice and guidance throughout the project were provided by D. Wrisley, G. Cvijanovich, F. Desk and R.H. Zimmerman. We wish to acknowledge D. Leahy, R. Shimps and J. Everidge for the analytical work. R. Moore and many of his people collaborated in the implementation of the process on a development line. We thank K. Platt for assistance with the computer modeling.

REFERENCES

1. R. Srinivasan, J. Vat. Sci. Technol. **Bl,** 923 (1983).

2. R. Srinivasan and V. Mayne-Barton, Appl. Phys. Lett. **41** ,576 (1982).

3. J. E. Andrew, P. E. Dyer, D. Forster, and P.' H. Key, Appl. Phys. Lett. **43** ,717 (1983).

4. R. Srinivasan, M. A. Smitic, and S. V. Babu, J. Appl. Phys. **59,** 3861 (1986).

5. G. Gorodestsky, T. G. Dazyaka, R. L. Melcher, and R. Srinivasan, Appl. Phys. Lett. **46,** 828 (1985).

6. G. Koren and J. T. C. Yeh, Appl. Phys. Lett. **44,** 1112 (1984).

7. K. Ogawa et al., Electrochemical Society Meeting, October 1987.

8. Lambda Physik Highlights, No. 2, December 1986.

9. J. Wrobel, A. Marchant, and D. Howe, Appl. Phys. Lett. **40,** 928 (1982).

10. J. R. Rowlette and D. Goetzinger, private communication,

11. G. Koren and J. T. C. Yeh, J. Appl. Phys. **56,** 2120 (1984).

12. H. Cole, Y. Liu, H. Philipp, and R. Guida, Mat. Res. Sot. Symp. Proc. **72,** 241 (1986).

13. H. Nine, M. Nakano, S. Negano, A. Yake, and T. Miki, Appl.Phys.Lett. **55,** 510 (1989).

14. Handbook of Optical Constants of Solids, ed. by E.D. Palik, Academic Press (1985).

15. American Institute of Physics Handbook, Third Edition, McGraw Hill (1972).

Jeff Wu is a Member of the Technical Staff in the Technology Group of AMP Incorporated in Winston-Salem, North Carolina.

Dr. Wu received a B.S. in electrical engineering from National Taiwan University in 1968 and a Ph.D. in engineering from Brown University in 1977. Before joining AMP in 1979, he was acting manager of the Solar Cell Department of the McGraw Edison Company. His areas of expertise include thin-film technology, solar cell technology, and laser materials processing. He holds six U.S. patents and one foreign patent; he has published three papers. Dr. Wu is a member of IEEE and Sigma Xi.

Richard T. Williams is the Reynolds Professor of Physics at Wake Forest University in Winston-Salem, North Carolina.

Dr. Williams holds a B.S. (1968) from Wake Forest University and an M.A. (1971) and a Ph.D. (1974) from Princeton University. He was the head of UV Technology Section, Optics Probes in the Naval Research Laboratory before joining Wake Forest in 1985. His current research areas include ultrafast spectroscopy, laser materials, and high-temperature superconductivity. He has written 58 papers, holds seven patents, and is a consultant to AMP and to the Naval Research Laboratory.

Anqi Wu is a graduate student in the Department of Physics at Wake Forest University in Winston-Salem, North Carolina.

Mr. Wu received his B.S. from Beijing Normal University in 1982. He has published one paper and is a member of the American Physical Society, Material Research Society, and Sigma Xi.

Hanli Liu is a graduate student in the Department of Physics at Wake Forest University in Winston-Salem, North Carolina.

Ms. Liu received a B.S. in physics from Beijing Normal University in 1983 and an M.S. in physics from Wake Forest University in 1990. She has written three papers.

Charles W. Himes is a graduate student in the Department of Physics at Wake Forest University in Winston-Salem, North Carolina.

Mr. Himes received his B.S. from the University of North Carolina at Greensboro in 1990.